Journal of Computational Physics 300 (2015) 574–591

Contents lists available at ScienceDirect

Journal of Computational Physics

www.elsevier.com/locate/jcp

Finite difference approximations of multidimensional convection–diffusion–reaction problems with small diffusion on a special grid

Adem Kaya [a,*], Ali Sendur [b]

[a] Department of Mathematics, Izmir Institute of Technology, 35430 Izmir, Turkey
[b] Department of Mathematics Education, Alanya Alaaddin Keykubat University, 07490 Antalya, Turkey

ARTICLE INFO

Article history:
Received 26 September 2014
Received in revised form 30 July 2015
Accepted 4 August 2015
Available online 10 August 2015

Keywords:
Finite Difference Methods
Finite Element Methods
Convection–diffusion–reaction
Non-uniform grid
Singular perturbation

ABSTRACT

A numerical scheme for the convection–diffusion–reaction (CDR) problems is studied herein. We propose a finite difference method on a special grid for solving CDR problems particularly designed to treat the most interesting case of small diffusion. We use the subgrid nodes in the Link-cutting bubble (LCB) strategy [5] to construct a numerical algorithm that can easily be extended to the higher dimensions. The method adapts very well to all regimes with continuous transitions from one regime to another. We also compare the performance of the present method with the Streamline-upwind Petrov–Galerkin (SUPG) and the Residual-Free Bubbles (RFB) methods on several benchmark problems. The numerical experiments confirm the good performance of the proposed method.

1. Introduction

It is well known that the exact solution of the convection–diffusion–reaction (CDR) problems may contain layers when some problem parameters are too big compared to others. Typically in this model problem, but also in real fluid flow simulation, the major difficulty is the appearance of the nonphysical oscillations that pollute the numerical solution in the whole domain, while the exact solution only shows boundary or internal layers. To overcome this difficulty, several numerical recipes have been evolved over the years [32,33] among them a commonly used one is the finite difference method [1,11,13,27]. The early numerical solutions were obtained by using standard finite difference scheme of upwind and centered type on a uniform mesh and then refining the mesh more and more in order to capture the boundary/internal layers. However, even for 1-D problems those methods were inefficient and accurate solutions could not be obtained for higher dimensions. In [3], Bakhvalov considered an upwind difference scheme on a layer-adapted meshes. They are very fine inside the boundary layer and coarse outside. Moreover, in 1990s the Russian mathematician Shishkin showed that one could use a simpler piecewise uniform mesh to obtain reasonable approximations [14,36]. This idea has been propagated throughout the 1990s by a group of Irish mathematicians: Miller, O'Riordan and Farrell [29]. The simplicity of those approaches is due to the use of equidistant subintervals on both sides of a transition point and this property is considered to be one of its major attractions. However, it requires the precise location of the layer structure a priori.

* Corresponding author.
E-mail addresses: ademkaya@iyte.edu.tr (A. Kaya), alisendur@akdeniz.edu.tr (A. Sendur).

http://dx.doi.org/10.1016/j.jcp.2015.08.007
0021-9991/

Another major approach to obtain reasonable approximations for the CDR problem is the finite element method (FEM) [2,14,21]. The most successful classes of FEMs for treating convection-dominated problems are achieved by the stabilized formulations [16,18,19,22,24,37]. As an important and well-known example to that class, the Streamline-Upwind/Petrov–Galerkin (SUPG) method could be mentioned that is first proposed by Hughes and his co-workers [10]. SUPG method is based on enlarging the variational formulation by adding diffusion in the streamline direction while preserving the consistency. Despite the success of SUPG method, the need for the proper choice of stabilizing parameter is considered as a major drawback of the method. Regarding that fact, intrinsically stable methods such as the Residual-Free Bubbles (RFB) method has been developed [2,4,8,9,17]. The main idea underlying the RFB method is to enrich the finite element space, instead of a modification of the variational formulation, by a set of special functions, so called bubble functions. A thorough comparison of some of these methods can be found in [12,28,38]. However, it requires to solve a local differential equation which may not be easier than to solve the original one [15]. That observation has motivated the introduction of a further option so-called the Pseudo Residual-free Bubble (PRFB) method which approximates the bubble functions on a specially chosen subgrid [6,7,31,34,35]. Roughly speaking, such grid points can be constructed by minimizing the residual of a local differential equation with respect to L_1 norm so that small scale-effect of the exact solution could be accurately represented in the numerical approximation through the use of those approximate bubble functions [34]. Alternatively, the Link-Cutting Bubbles (LCB) method that is based on the plain Galerkin variational formulation on a special grid was proposed by Brezzi et al. in [5] and it could be viewed as a similar, yet interesting option for another stable discretization in 1D. However, extension of that strategy to the higher dimensions is not a trivial task. It is also worth mentioning that the convection–diffusion–reaction equations with positive and negative reactive terms (source terms) is considered in [23].

The algorithm investigated in this work is motivated by a simple splitting of the 2-D CDR equation into the sum of two 1-D equations [25]. It combines the ideas of the LCB method in [5] and finite difference methods (FDM) on special meshes. Indeed, we will use the subgrid nodes in the LCB strategy and construct a FDM for solving CDR problems. Thus, we develop a numerical recipe for solving CDR problems that is simple to use, easy to implement and can easily be extended to higher dimensions. We also compare the performance of the present method with the well-known SUPG and RFB methods on several benchmark problems. A wide range of problem parameters has been examined on both structured and unstructured meshes and the corresponding numerical results are presented.

The layout of the paper is as the following. We briefly recall the basic idea of the LCB method in Section 2. In Section 3, we describe the details of the numerical method proposed and discuss the generation of the grid for two dimensional problem. Finally, we perform the numerical tests for several benchmark problems in both 2D and 3D in Section 4.

2. A review of the Link-Cutting Bubble strategy in [5]

We consider the following linear elliptic convection–diffusion–reaction problem on a unit interval $I = (0, 1)$

$$\begin{cases} \mathcal{L}u = -\epsilon u'' + \beta u' + \sigma u = f(x) \text{ on } I, \\ u(0) = u(1) = 0, \end{cases} \tag{1}$$

under the assumptions that the diffusion coefficient ϵ is positive constant, convection field β and reaction field σ are non-negative constants. We denote the decomposition of I into subintervals by $T_h = \{K_k\}$ where $K_k = (x_{k-1}, x_k)$, $k = 1, \ldots, N$ and the size of the interval K_k by $h_k = x_k - x_{k-1}$.

The Link-Cutting Bubble (LCB) strategy introduced in [5] is designed for one-dimensional convection–diffusion–reaction problem and it aims to mimic the stabilizing effect of Residual Free Bubbles (RFB), without actually computing them. To do this, we choose a suitable subgrid made of two points inside each element and we take the bubbles which are piecewise linear on the subgrid. The strategy for choosing the subgrid is as follows: Consider a typical element, (x_1, x_2), then the subgrid nodes are obtained by adding two extra nodes, say z_1 and z_2 satisfying $x_1 < z_1 < z_2 < x_2$ and

$$\begin{aligned} z_1 - x_1 &= \min\left\{ h_k - 2(x_2 - z_2), \frac{3\beta + \sqrt{9\beta^2 + 24\epsilon\sigma}}{2\sigma} \right\} \\ x_2 - z_2 &= \min\left\{ \frac{h_k}{3}, \frac{-3\beta + \sqrt{9\beta^2 + 24\epsilon\sigma}}{2\sigma} \right\}. \end{aligned} \tag{2}$$

Once the subgrid nodes are constructed, the LCB strategy works as the standard Galerkin method with piecewise linear basis functions on augmented mesh. For the behavior of the scheme at various regimes, see [5].

3. The construction of the numerical method

In this section, using the subgrid nodes in the LCB strategy, we propose a numerical algorithm for solving convection–diffusion–reaction (CDR) problems which can easily be extended to the higher dimensional problems. Now, consider the following constant coefficient linear elliptic convection–diffusion–reaction problem in a polygonal domain Ω:

$$\begin{cases} -\epsilon\left(\frac{\partial^2 u}{\partial x^2}+\frac{\partial^2 u}{\partial y^2}\right)+b.\left(\frac{\partial u}{\partial x},\frac{\partial u}{\partial y}\right)+\sigma u=f(x,y) \text{ on } \Omega \\ u(x,y)=g \text{ on } \partial\Omega \end{cases} \tag{3}$$

under the assumptions that $\epsilon>0$, $b=(b_1,b_2)\neq 0$ and $\sigma\geq 0$. The problem (3) can be rewritten as,

$$\begin{cases} -\epsilon\left(\frac{\partial^2 u}{\partial x^2}\right)+b_1\left(\frac{\partial u}{\partial x}\right)+\sigma\frac{|b_1|}{|b_1|+|b_2|}u-\epsilon\left(\frac{\partial^2 u}{\partial y^2}\right)+b_2\left(\frac{\partial u}{\partial y}\right)+\sigma\frac{|b_2|}{|b_1|+|b_2|}u \\ \quad=\frac{|b_1|}{|b_1|+|b_2|}f(x,y)+\frac{|b_2|}{|b_1|+|b_2|}f(x,y) \text{ on } \Omega \\ u(x,y)=g \text{ on } \partial\Omega. \end{cases} \tag{4}$$

Next, we consider the problem (3) as a sum of the following 1-D problems,

$$\begin{cases} -\epsilon\left(\frac{d^2 u}{dx^2}\right)+b_1\left(\frac{du}{dx}\right)+\sigma\frac{|b_1|}{|b_1|+|b_2|}u=\frac{|b_1|}{|b_1|+|b_2|}f, \\ -\epsilon\left(\frac{d^2 u}{dy^2}\right)+b_2\left(\frac{du}{dy}\right)+\sigma\frac{|b_2|}{|b_1|+|b_2|}u=\frac{|b_2|}{|b_1|+|b_2|}f. \end{cases} \tag{5}$$

We start by employing the standard Galerkin finite element method with piecewise linear basis functions to the problem (1) on uniform meshes which can be written in the following form:

$$\begin{cases} -\epsilon\frac{u_{j+1}-2u_j+u_{j-1}}{h^2}+\beta\frac{u_{j+1}-u_{j-1}}{2h}+\sigma\frac{u_{j+1}+4u_j+u_{j-1}}{6}=\frac{f_{j-1}+4f_j+f_{j+1}}{6}, \quad j=1,\ldots,N-1 \\ u_0=u_N=0 \end{cases}$$

where h denotes the size of each interval and u_j denotes the numerical approximation to $u(x_j)$. The corresponding numerical scheme on a nonuniform mesh reads:

$$\begin{cases} -\epsilon\frac{u_{j+1}}{h_2}+\epsilon\frac{u_j}{h_2}+\epsilon\frac{u_j}{h_1}-\epsilon\frac{u_{j-1}}{h_1}+\beta\frac{u_{j+1}-u_{j-1}}{2}+\sigma\frac{h_2u_{j+1}+2h_2u_j+2h_1u_j+h_1u_{j-1}}{6} \\ \quad=\frac{h_2f_{j+1}+2h_2f_j+2h_1f_j+h_1f_{j-1}}{6}, \\ u_0=u_N=0 \qquad\qquad j=1,\ldots,N-1 \end{cases} \tag{6}$$

where $h_1=x_j-x_{j-1}$ and $h_2=x_{j+1}-x_j$. Now, employing the finite difference method in (6) to the equations in (5) and summing up those approximations, we get the following finite difference approximation for the problem (3),

$$\begin{cases} -\epsilon\frac{u_{i+1,j}}{n_2}+\epsilon\frac{u_{i,j}}{n_2}+\epsilon\frac{u_{i,j}}{n_1}-\epsilon\frac{u_{i-1,j}}{n_1}+b_1\frac{u_{i+1,j}-u_{i-1,j}}{2}+\sigma\frac{|b_1|}{|b_1|+|b_2|}\frac{n_2u_{i+1,j}+2n_2u_{i,j}+2n_1u_{i,j}+n_1u_{i-1,j}}{6} \\ \quad-\epsilon\frac{u_{i,j+1}}{m_2}+\epsilon\frac{u_{i,j}}{m_2}+\epsilon\frac{u_{i,j}}{m_1}-\epsilon\frac{u_{i,j-1}}{m_1}+b_2\frac{u_{i,j+1}-u_{i,j-1}}{2}+\sigma\frac{|b_2|}{|b_1|+|b_2|}\frac{m_2u_{i,j+1}+2m_2u_{i,j}+2m_1u_{i,j}+m_1u_{i,j-1}}{6} \\ =\frac{|b_1|}{|b_1|+|b_2|}\frac{n_2f_{i+1,j}+2n_2f_{i,j}+2n_1f_{i,j}+n_1f_{i-1,j}}{6}+\frac{|b_2|}{|b_1|+|b_2|}\frac{m_2f_{i,j+1}+2m_2f_{i,j}+2m_1f_{i,j}+m_1f_{i,j-1}}{6} \end{cases}$$

where $n_2=x_{i+1}-x_i$, $n_1=x_i-x_{i-1}$, $m_2=y_{i+1}-y_i$, $m_1=y_i-y_{i-1}$.

Remark 1. We note that splitting the 2-dimensional CDR equation into the two 1-dimensional CDR equations is not arbitrary and it is same with the one in [25]. We also note that, convergence tests in the L_2 norm confirm that the present splitting is the optimal one among different possibilities that we considered.

Moreover, it is known that the Link-cutting bubble strategy in [5] is viewed as a standard Galerkin method on augmented mesh, therefore we do not consider the finite difference analogue of the bubble condensation. Indeed, the evaluation of the additional unknowns is clearly explained in [25].

3.1. Derivation of the finite difference scheme on nonuniform grid with Taylor Series expansion

We start with considering the following Taylor Series expansions,

$$u(x+h_2)=u(x)+h_2u'(x)+\frac{h_2^2}{2}u''(x)+O(h_2^3), \tag{7}$$

$$u(x-h_1)=u(x)-h_1u'(x)+\frac{h_1^2}{2}u''(x)+O(h_1^3). \tag{8}$$

One can get the first derivative approximation from (7) and (8) easily as follows;

$$u'(x)\approx\frac{u_{j+1}-u_{j-1}}{h_1+h_2}. \tag{9}$$

Dividing both sides of the equations (7) by h_2 and (8) by h_1 and adding we get

$$\left(\frac{h_1+h_2}{2}\right)u''(x)=\frac{u(x+h_2)}{h_2}-\frac{u(x)}{h_2}-\frac{u(x)}{h_1}+\frac{u(x-h_1)}{h_1}+O(h_1^2)+O(h_2^2). \tag{10}$$

Dividing both sides of equation (10) by $(h_1+h_2)/2$ we get the second derivative approximation as follows;

$$u''(x)\approx\left(\frac{u_{j+1}}{h_2}-\frac{u_j}{h_2}-\frac{u_j}{h_1}+\frac{u_{j-1}}{h_1}\right)\left(\frac{2}{h_1+h_2}\right). \tag{11}$$

Multiplying equations (7) by h_2 and (8) by h_1 we get

$$h_2u(x+h_2)=h_2u(x)+O(h_2^2), \tag{12}$$

$$h_1u(x-h_1)=h_1u(x)+O(h_1^2). \tag{13}$$

Adding (12) and (13) and dividing by h_1+h_2 one can derive the following approximation

$$u(x)\approx\frac{h_2u_{j+1}+h_1u_{j-1}}{h_1+h_2}. \tag{14}$$

From equations (12) and (13) we can write

$$h_2u(x+h_2)+2h_2u(x)=3h_2u(x)+O(h_2^2), \tag{15}$$

$$h_1u(x-h_1)+2h_1u(x)=3h_1u(x)+O(h_1^2). \tag{16}$$

Adding equations (15) and (16) and dividing by $3(h_1+h_2)$ we get the following approximation

$$u(x)\approx\frac{h_2u_{j+1}+2h_2u_j+2h_1u_j+h_1u_{j-1}}{3(h_1+h_2)}. \tag{17}$$

Approximating u'' by (11), u' by (9), u and source function f by (17) for the 1-D convection–diffusion–reaction equation and multiplying with h_1+h_2 and dividing by 2 we get the following finite difference approximation

$$\begin{aligned}&-\epsilon\frac{u_{j+1}}{h_2}+\epsilon\frac{u_j}{h_2}+\epsilon\frac{u_j}{h_1}-\epsilon\frac{u_{j-1}}{h_1}+\beta\frac{u_{j+1}-u_{j-1}}{2}+\sigma\frac{h_2u_{j+1}+2h_2u_j+2h_1u_j+h_1u_{j-1}}{6}\\&=\frac{h_2f_{j+1}+2h_2f_j+2h_1f_j+h_1f_{j-1}}{6}.\end{aligned} \tag{18}$$

We note that the scheme in (18) can be viewed as the finite difference correspondence of standard finite element method with piecewise linear basis functions. It is easy to see from the derivation that the finite difference scheme (18) is second order accurate, in the sense $O(h_1^2)+O(h_2^2)$. If we approximate the terms of the CDR equation in 2-D with finite difference approximations (11), (9) and (17) we get a first order approximation, in the sense $O(\frac{n_1^2}{n_1+n_2})+O(\frac{n_2^2}{n_1+n_2})+O(\frac{m_1^2}{m_1+m_2})+O(\frac{m_2^2}{m_1+m_2})$. Assuming $m_1+m_2=n_1+n_2$ and splitting the reaction term and source function as done before and multiplying with $(m_1+m_2)/2$ we get the finite difference approximation obtained by the decomposition which is second order accurate, in the sense $O(n_1^2)+O(n_2^2)+O(m_1^2)+O(m_2^2)$. This justifies that the decomposition can be done with the above finite difference approximations under the assumption that $m_1+m_2=n_1+n_2$. Numerical tests show that even with very distorted mesh the decomposition can be applied.

3.2. The generation of the grid for 2-D problems

We start with an initial discretization of the domain that can be structured or unstructured. A five point stencil of the initial discretization is presented in Fig. 1 (left). Augmented discretization is obtained by adding 24 sub-grid nodes into the initial stencil as shown in Fig. 1 (right). The x-coordinates of the sub-grid nodes are determined by applying the Link-cutting bubble strategy to the first equation in (5) either in the interval $(x_{i-1,j}, x_{i,j})$ or in $(x_{i,j}, x_{i+1,j})$ according to their projection onto the x-axis. Similarly, y-coordinates are determined by applying the same procedure to the second equation in (5) either in the interval $(y_{i,j-1}, y_{i,j})$ or in $(y_{i,j}, y_{i,j+1})$ according to their projection onto the y-axis. Before we outline the construction of the algorithm, it is worth mentioning that the present method can also be applied to the complex domains.

Now, let us denote the number of grid points of initial discretizations in x and y-directions by N and M respectively; the points in the initial discretization by $(x_{i,j}, y_{i,j})$ in a rectangular domain where $i=1,\ldots,N$, $j=1,\ldots,M$. The second discretization which we will refer to as modified discretization, is constructed by using the subgrid nodes in the Link-cutting bubble strategy in x and y-direction separately and the modified discretization consists of $(3N-2)\times(3M-2)$ points. Algorithm 1 summarizes the procedure in 2-D case.

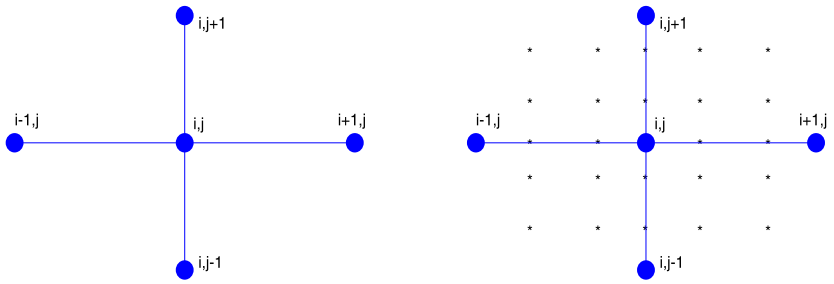

Fig. 1. Five point initial stencil (left) and its modified version (right) in 2-D.

Algorithm 1: Discretization of the domain in 2-D in a rectangular domain.

Data: $(x_{i,j},\ y_{i,j})$ for $i = 1, \ldots, N,\ j = 1, \ldots, M$ and the problem parameters.
Result: $(x'_{i,j},\ y'_{i,j})$ where $i = 1, \ldots, 3N-2$ and $j = 1, \ldots, 3M-2$.
`Step 1:` Do an initial discretization that can be structured or unstructured.
`Step 2:` The derivation of $x'_{i,j}$,
Use the problem parameters of the first equation in (5): $\epsilon = \epsilon$, $\beta = \mid b_1 \mid$ and $\sigma = \sigma \frac{|b_1|}{|b_1|+|b_2|}$;
for *j=1* **to** $3M-2$ **do** ;
for *i=1* **to** $N-1$ **do** ;
Using the equation (2), calculate z_1 and z_2 in $(x_{i+1,j}, x_{i,j})$ to get
$x'_{3i,j} = z_2 \qquad x'_{3i-1,j} = z_1 \qquad x'_{3i-2,j} = x_{i,j} \qquad x'_{3N-2,j} = x_{N,j}$.
`Step 3:` The derivation of $y'_{i,j}$;
Use the problem parameters of the second equation in (5): $\epsilon = \epsilon$, $\beta = \mid b_2 \mid$ and $\sigma = \sigma \frac{|b_2|}{|b_1|+|b_2|}$;
for *j=1* **to** $3N-2$ **do** ;
for *i=1* **to** $M-1$ **do** ;
Using the equation (2), calculate z_1 and z_2 in $(y_{j,i+1}, y_{j,i})$ to get
$y'_{j,3i} = z_2 \qquad y'_{j,3i-1} = z_1 \qquad y'_{j,3i-2} = y_{j,i} \qquad y'_{j,3M-2} = y_{j,M}$.

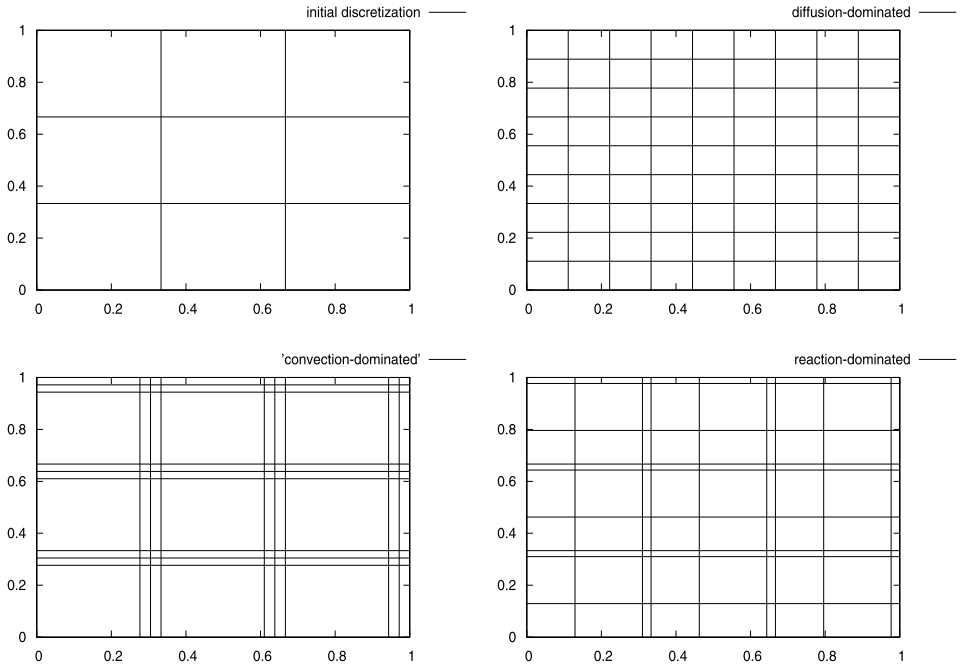

Fig. 2. Initial discretization and modified discretizations in three different regimes for $N = M = 4$.

In Fig. 2, we first consider the diffusion-dominated case by setting

$$\epsilon = 1,\ (b_1, b_2) = (\cos 45^\circ, \sin 45^\circ),\ \sigma = 10^{-6}$$

and then we consider the convection-dominated case by setting

$$\epsilon = 0.01,\ (b_1, b_2) = (\cos 45^\circ, \sin 45^\circ),\ \sigma = 10^{-6}$$

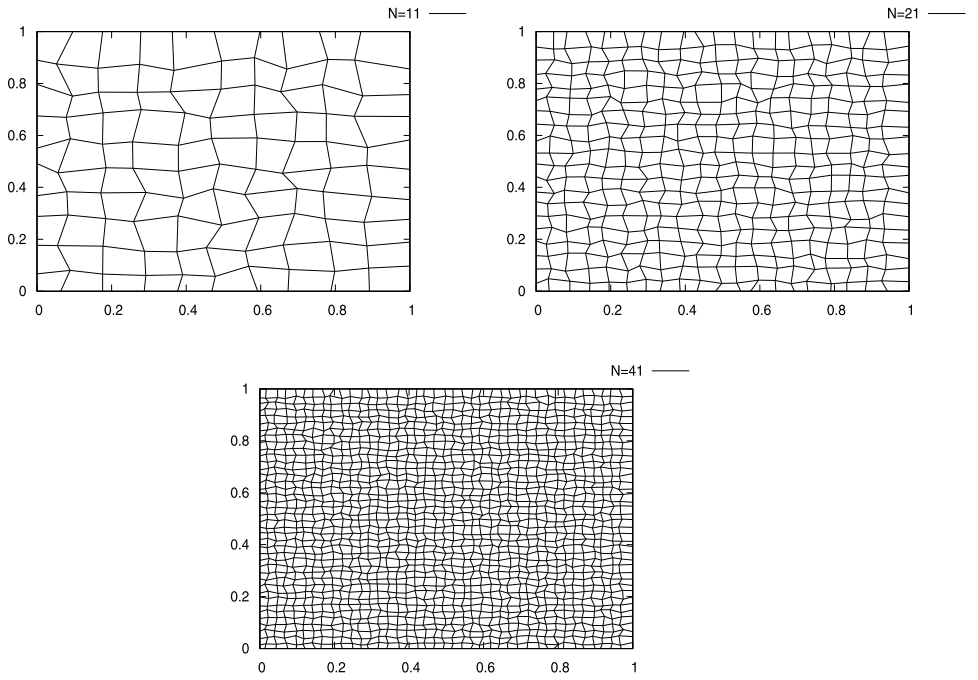

Fig. 3. Initial discretizations of unstructured meshes used in the discretization of the problem domain.

and finally we consider the reaction-dominated case by setting

$$\epsilon = 0.01,\ (b_1, b_2) = (\cos 45^\circ, \sin 45^\circ),\ \sigma = 10$$

and display a sample of initial discretization and modified discretizations for different problem regimes.

Finally, we recall that the problem is first solved on augmented grid and then the subgrid nodes are excluded to simulate the numerical results.

Remark 2. We note that, it is easy to extend the stabilization technique above to the convection–diffusion–reaction problems in higher dimensions by an analogy to the 2-D case in which one needs to split the n-dimensional CDR equation into the sum of "n" 1-dimensional equations and follow the discussions in the previous lines.

We also note that, in 3-D domains, 124 sub-grid nodes are added into the initial stencil to derive the augmented discretization and the coordinates of the sub-grid nodes are determined by applying the same procedure as we did in the 2-D case (see [26] for details).

4. Numerical results

In this section, we report some numerical experiments to illustrate the performance of the present method for a wide range of problem parameters, especially in the interesting case of small diffusion which corresponds to the convection-dominated or reaction-dominated regimes on both structured and unstructured grids. We compare the proposed method with the well-known stabilized finite element methods: the SUPG and the RFB methods. The Fig. 3 displays three types of initial discretizations of unstructured grids for $N = 11, 21, 41$ where N denotes the number of nodes in x and y-direction on initial discretization throughout this section. We also report the errors in the L_2 norm. The dimensionless numbers that characterize the solution are

$$Pe = \frac{|b|h}{2\epsilon} \quad \text{Element Peclet Number}$$

$$Da = \frac{\sigma h}{|b|} \quad \text{Element Damkohler Number}$$

where h is the element size.

4.1. Numerical experiments for 2-D CDR problem

4.1.1. Experiment 1: an example with analytical solution

In the convergence analysis, we consider a simple problem on a unit square that can be solved analytically and subject to the following boundary conditions

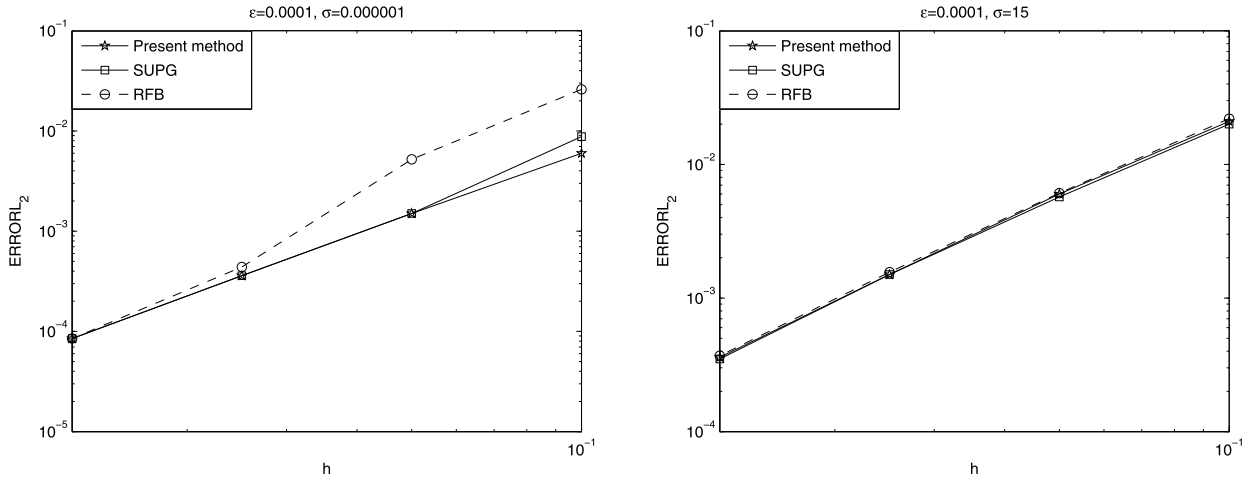

Fig. 4. The errors in the L_2 norm for $\epsilon = 10^{-4}$ and two different values of σ.

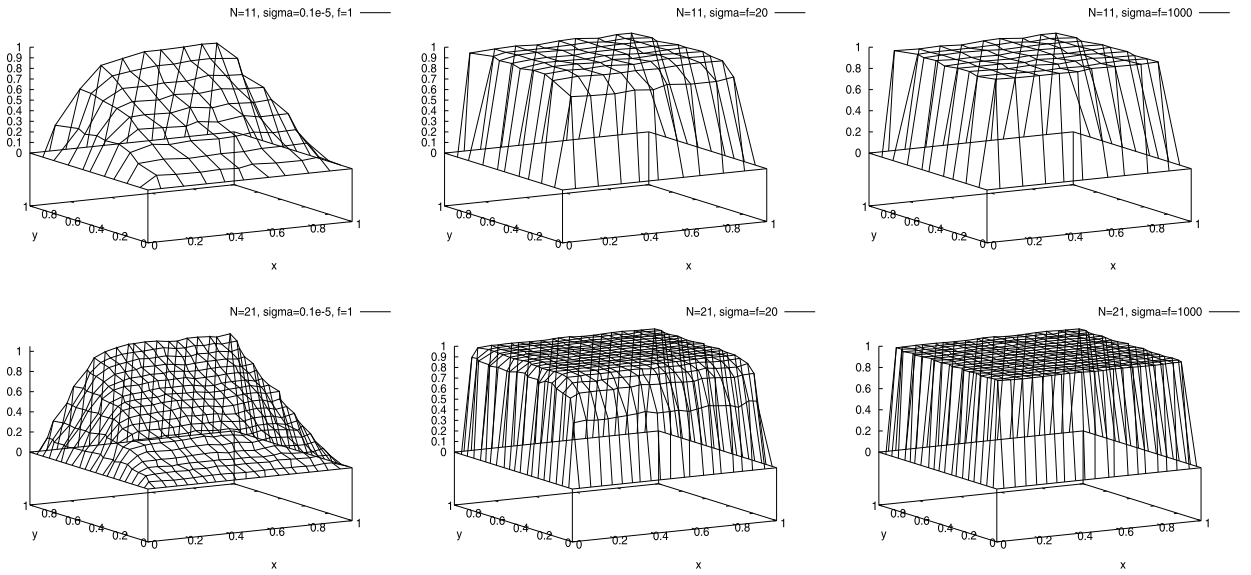

Fig. 5. Numerical approximations obtained with unstructured meshes when $\epsilon = 10^{-6}$, $\sigma = 10^{-6}, 20, 1000$, $f = 1, 20, 1000$.

$$u = \begin{cases} 0, & \text{if } y = 0\,,\ 0 \le x \le 1, \\ 0, & \text{if } x = 1\,,\ 0 \le y \le 1, \\ 0, & \text{if } y = 1\,,\ 0 \le x \le 1, \\ \sin(\pi y), & \text{if } x = 0\,,\ 0 \le y \le 1. \end{cases}$$

We set $\beta = (1,\ 0)$ and $f(x) = 0$ in Ω. Using the separation of variables, the exact solution is given by:

$$u(x, y) = \frac{e^{x/2\epsilon}\ \sinh\left(-m(1-x)\right)\ \sin(\pi y)}{\sinh\left(-m\right)} \quad \text{where} \quad m = \sqrt{1 + 4\epsilon(\epsilon\pi^2 + \sigma)}/2\epsilon.$$

Next, we take a set of uniform grid with grid sizes $h = 0.1, 0.05, 0.025, 0.0125$, both in x and y directions. In Fig. 4, we present the log–log plots of errors in the L_2 norm for different values of ϵ and σ. The results show that the proposed method achieves slightly better performance than the SUPG and the RFB method. Moreover, the improvement is apparent for each method as the mesh is refined and the expected convergence rates are achieved.

4.1.2. Experiment 2

We consider an example with homogeneous Dirichlet boundary conditions, yet the source function is non-zero (see [12]). We first take a set of unstructured mesh with $N = 11, 21$. We set $\epsilon = 10^{-6}$, $(b_1, b_2) = (\cos 72°, \sin 72°)$ and present elevation plots of the solutions obtained with the present method for various values of reaction ($\sigma = 10^{-6}, 20, 1000$) with $f = 1, 20, 1000$ in Fig. 5.

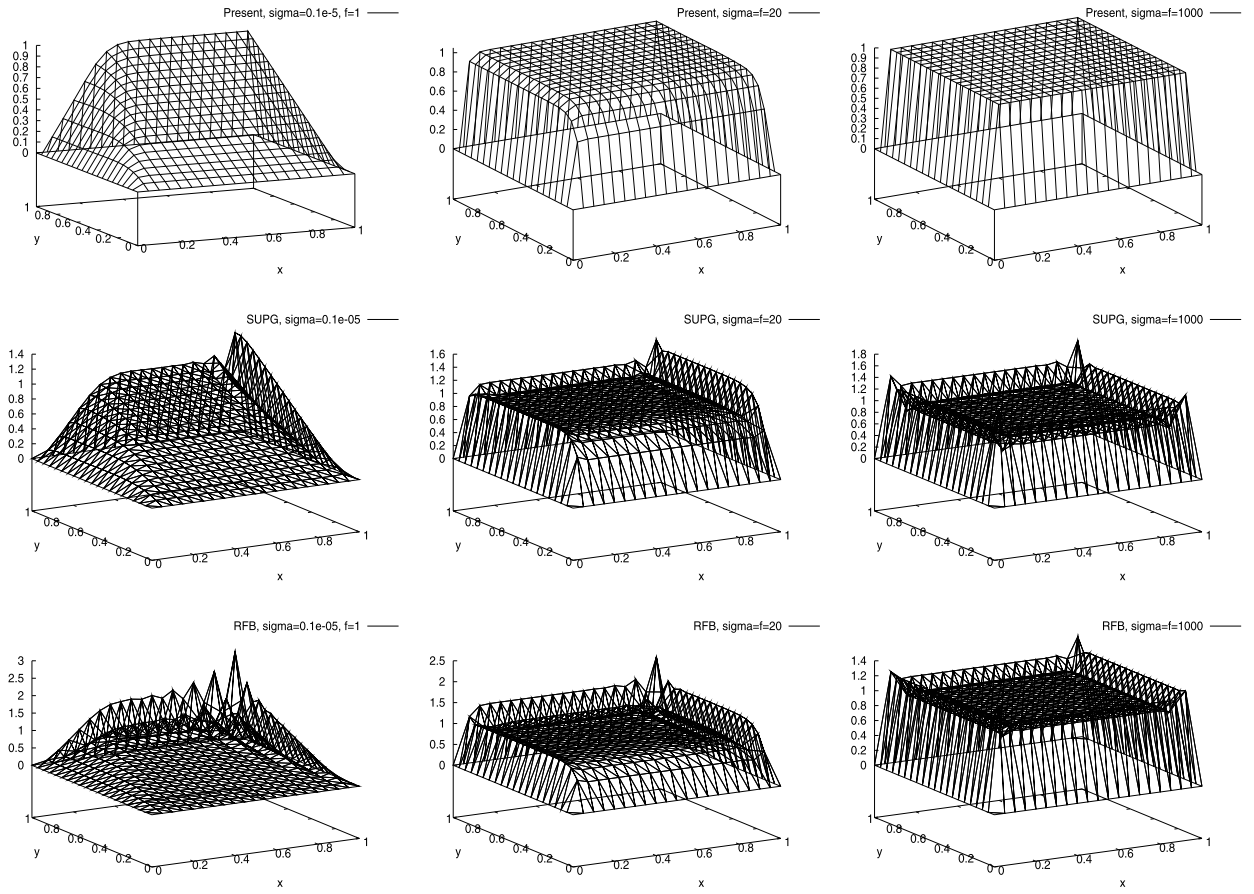

Fig. 6. Numerical approximations obtained with structured mesh when $\epsilon = 10^{-6}$, $\sigma = 10^{-6}, 20, 1000$, $f = 1, 20, 1000$ and $N = 21$ for which $Pe = 25 \times 10^3$, $Da = 0.5 \times 10^{-7}$ (first column), $Da = 1$ (second column) and $Da = 50$ (third column).

Next, we consider the same problem parameters on a structured mesh with $N = 21$ and present elevation plots of the numerical approximations obtained with SUPG, RFB and the present method in Fig. 6. The numerical experiments in Figs. 5–6 show that the present method is robust as the results are consistent with the physical configuration of the problem on both structured and unstructured meshes while the SUPG and RFB method produces slight oscillations at the outflow boundary.

4.1.3. Experiment 3

Next, we consider a test problem with homogeneous Dirichlet boundary conditions which is taken from [30]. We note that the exact solution has exponential layers at the outflow boundary ($x = 1$, y); characteristic boundary layers at (x, $y = 0$) and (x, $y = 1$). We first take a set of unstructured mesh with $N = 21$. We set $(b_1, b_2) = (1, 0)$, $\epsilon = 10^{-6}$, $f = 1$, $\sigma = 0$ and present elevation plots of the solutions obtained with the present method in Fig. 7.

Next, we consider the same problem parameters on a structured mesh and present elevation plots of the numerical approximations and corresponding contour plots obtained with the SUPG, RFB and the present method in Fig. 8. The numerical solution obtained with the SUPG method shows that the diffusion added in the streamline direction by the classical stabilization techniques, is not enough to eliminate the spurious oscillations as they are not completely removed from the approximation obtained with the RFB method.

4.1.4. Experiment 4

We consider the unit square subject to the following boundary conditions (see [35] for details):

$$u = \begin{cases} 0, & \text{if } y = 0\,, \ \ 0 \le x \le 1, \\ 0, & \text{if } x = 1\,, \ \ 0 \le x \le 1, \\ 1, & \text{if } y = 1\,, \ \ 0 \le x \le 1, \\ 1, & \text{if } x = 0\,, \ \ 0 \le y \le 1. \end{cases}$$

We set $\epsilon = 10^{-6}$, $(b_1, b_2) = (\cos 30^\circ, \sin 30^\circ)$, $\sigma = 10^3$ and $f = 0$. We first display the numerical results obtained with the present method on both structured/unstructured meshes with $N = 11$ in Fig. 9.

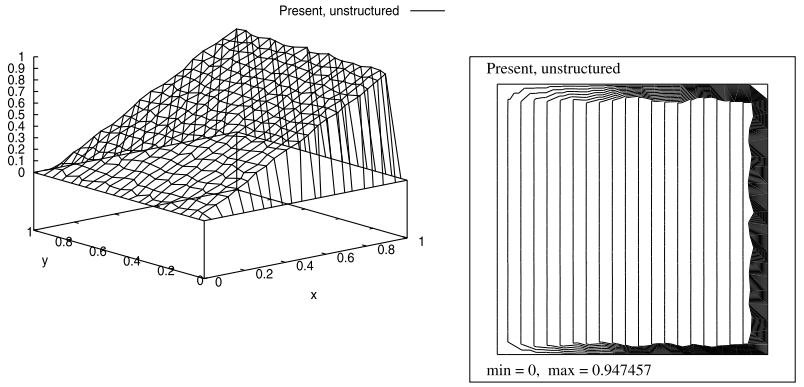

Fig. 7. Numerical approximation obtained with unstructured mesh when $\epsilon = 10^{-6}$, $(b_1, b_2) = (1, 0)$, $\sigma = 0$, $f = 1$, $N = 21$ and the corresponding contour plots.

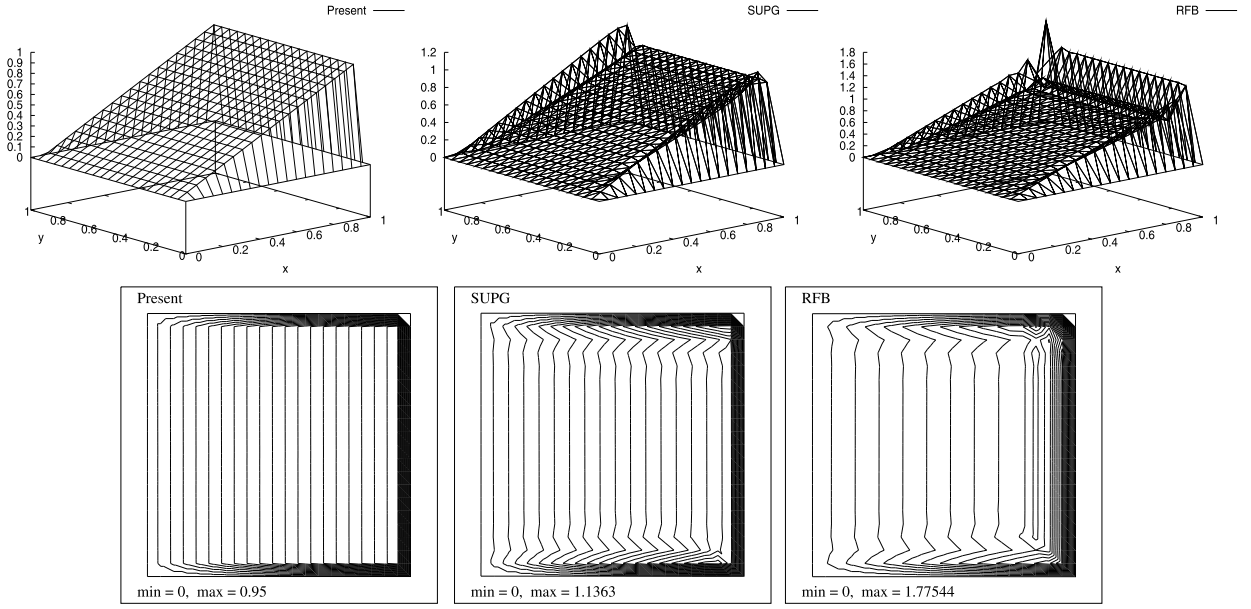

Fig. 8. Numerical approximations obtained with structured mesh when $\epsilon = 10^{-6}$, $(b_1, b_2) = (1, 0)$, $\sigma = 0$, $f = 1$ and $N = 21$ for which $Pe = 25 \times 10^3$, $Da = 0$.

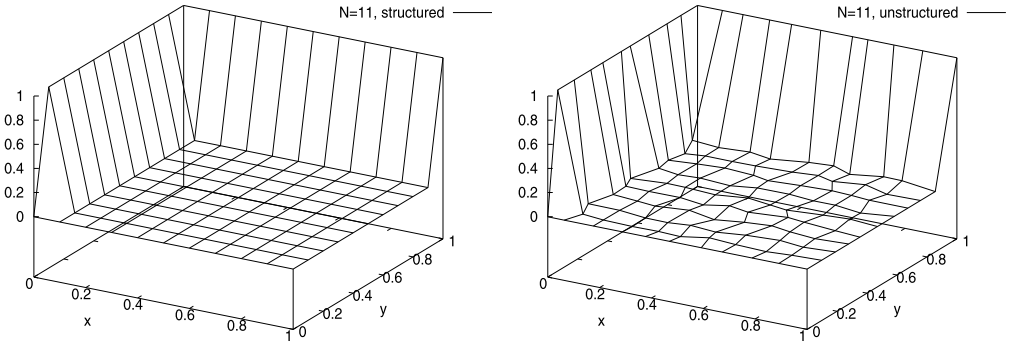

Fig. 9. Numerical approximations obtained with structured and unstructured meshes when $\epsilon = 10^{-6}$, $(b_1, b_2) = (\cos 30^\circ, \sin 30^\circ)$, $\sigma = 10^3$, $f = 0$ and $N = 11$ for which $Pe = 5 \times 10^4$, $Da = 10^2$.

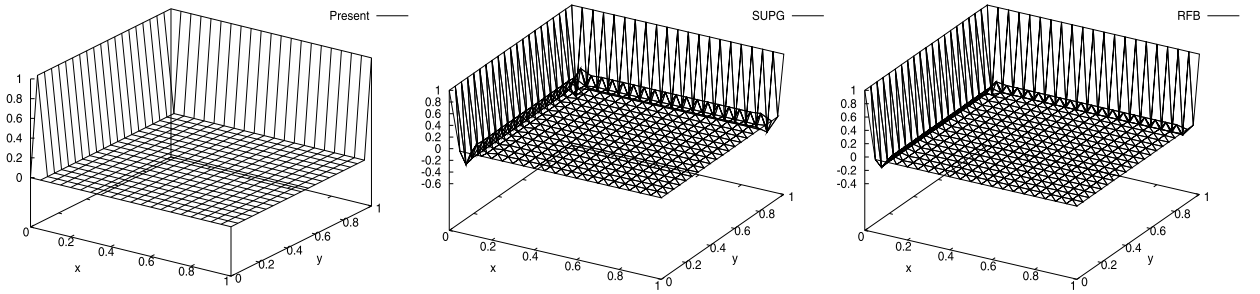

Fig. 10. Numerical approximations obtained with structured mesh when $\epsilon = 10^{-6}$, $(b_1, b_2) = (\cos 30^\circ, \sin 30^\circ)$, $\sigma = 10^3$, $f = 0$ and $N = 21$ for which $Pe = 25 * 10^3$, $Da = 50$.

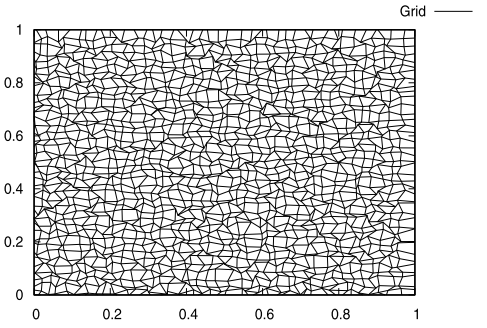

Fig. 11. Unstructured grid used in Test problem 5.

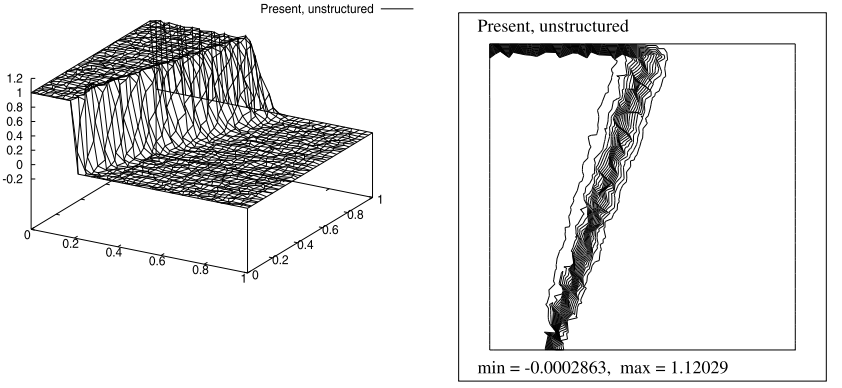

Fig. 12. Numerical approximation on unstructured mesh when $\epsilon = 10^{-6}$, $(b_1, b_2) = (\cos 72^\circ, \sin 72^\circ)$, $\sigma = 10^{-6}$, $f = 0$.

Next, we consider the same problem parameters on a structured mesh with $N = 21$ and present elevation plots of the numerical approximations obtained with the SUPG, RFB and the present method in Fig. 10. The present method captures the characteristic features of the exact solution while the SUPG and RFB method exhibits nonphysical oscillations.

4.1.5. Experiment 5: propagation of discontinuity in the boundary

Next, we consider the problem which is taken from [2] on unit square subject to the following boundary conditions:

$$u = \begin{cases} 1, & \text{if } y = 0, \ 0 \le x \le 0.2, \\ 0, & \text{if } y = 0, \ 0.2 < x \le 1, \\ 0, & \text{if } x = 1, \ 0 \le y \le 1, \\ 0, & \text{if } y = 1, \ 0 \le x \le 1, \\ 1, & \text{if } x = 0, \ 0 \le y \le 1. \end{cases}$$

This problem has exponential boundary layers at the outflow boundary and an internal layer. We first take a very distorted grid (see Fig. 11). We set $\epsilon = 10^{-6}$, $(b_1, b_2) = (\cos 72^\circ, \sin 72^\circ)$, $\sigma = 10^{-6}$, $f = 0$ and present elevation and contour plots of the solutions obtained with the present method in Fig. 12.

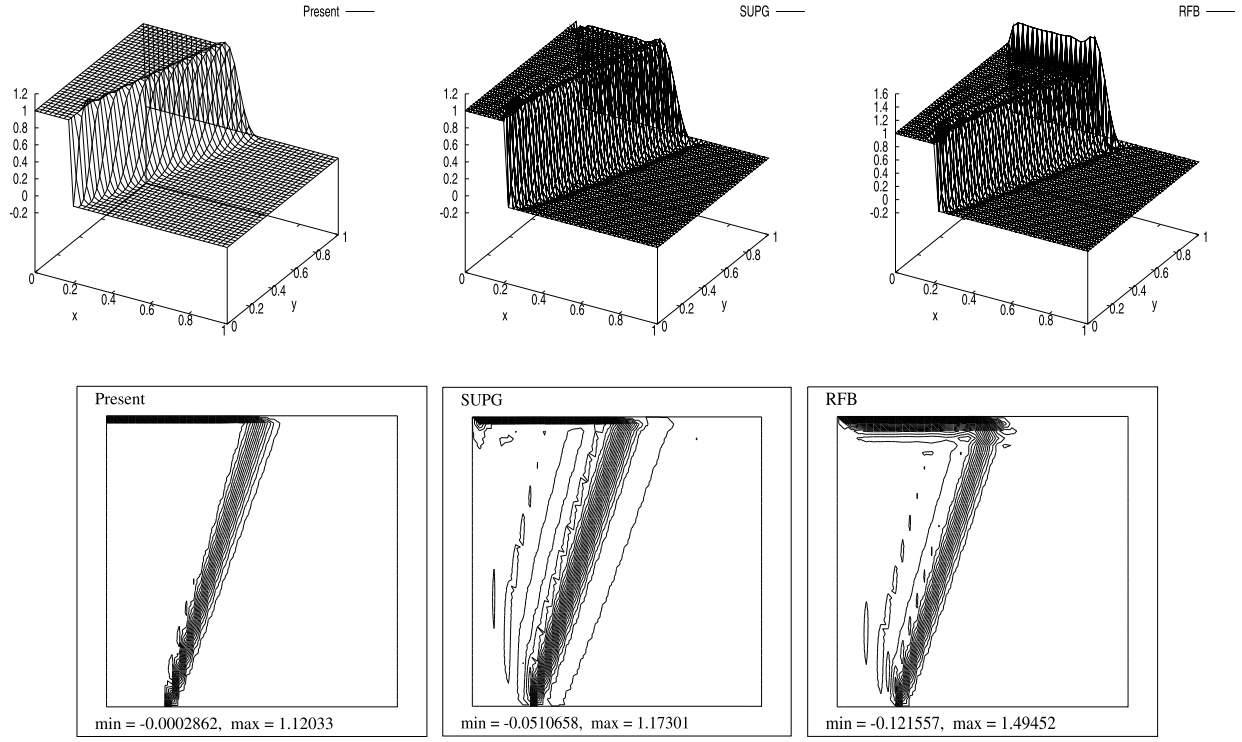

Fig. 13. Numerical approximations obtained with structured mesh when $\epsilon = 10^{-6}$, $(b_1, b_2) = (\cos 72^\circ, \sin 72^\circ)$, $\sigma = 10^{-6}$, $f = 0$ and $N = 41$ for which $Pe = 125 \times 10^2$, $Da = 4 \times 10^{-7}$.

Next, we consider the same problem parameters on a structured mesh and present the numerical approximations obtained with the SUPG, RFB and the present method in Fig. 13. The present method is able to handle both internal and boundary layers, and produce approximations consistent with the physical solution while the approximations generated by the SUPG and RFB methods possess spurious oscillations.

4.1.6. Experiment 6

We consider a more interesting discontinuous source function case which exhibits both internal and boundary layers. We take a set of unstructured mesh with $N = 21, 41$. We set

$$f(x, y) = \begin{cases} 800x^2, & \text{if, } 0 \le x \le 0.5, \\ -200x^2, & \text{if, } 0.5 < x \le 1 \end{cases}$$

$\epsilon = 10^{-6}$, $\sigma = 10^{-6}, 200$, $(b_1, b_2) = (0, 1)$ with homogeneous Dirichlet boundary conditions and display the numerical results in the Fig. 14. The plots show that the numerical approximation obtained with present method captures the characteristic features of the exact solution even on coarse mesh.

4.1.7. Experiment 7: an example on a complex domain

Next, we consider another interesting problem whose domain is defined as

$$(x = 0,\ 0 \le y \le 1),\ (0 \le x \le \cos(0.435\pi),\ y = 1),\ (0 \le x \le 1,\ y = 0),\ (x = \cos(0.435\pi y),\ 0 \le y \le 1)$$

and a square with edge length 0.157 and center $(0.236, 0.236)$. We will first consider homogeneous Dirichlet boundary conditions. We set $\epsilon = 10^{-8}$, $(b_1, b_2) = (\cos 20^\circ, \sin 20^\circ)$, $\sigma = 10^{-6}, 20, 1000$ with $f = 1, 20, 1000$. The computational grid is obtained by taking 396 nodes. The numerical results for the present method are reported in the Fig. 15. We observe that numerical solutions are non-oscillatory and are in good agreement with the physics of the problem parameters.

Next we consider non-homogeneous Dirichlet boundary conditions on some part of the domain which exhibits sharp layers at inflow boundary of the square and at outflow boundaries. We set $u = 1$ on $(x = 0,\ 0 \le y \le 1)$ and $(0 \le x \le 1,\ y = 0)$ and $u = 0$ on the rest of the boundary. We take $\epsilon = 10^{-8}$, $(b_1, b_2) = (\cos 20^\circ, \sin 20^\circ)$, $\sigma = 10^{-6}$ with $f = 0$. Fig. 16 shows that the proposed method effectively captures the layers. It seems that the present method is quite robust and effective algorithm in the numerical approximation of the convection–diffusion–reaction equations even the domain is complex.

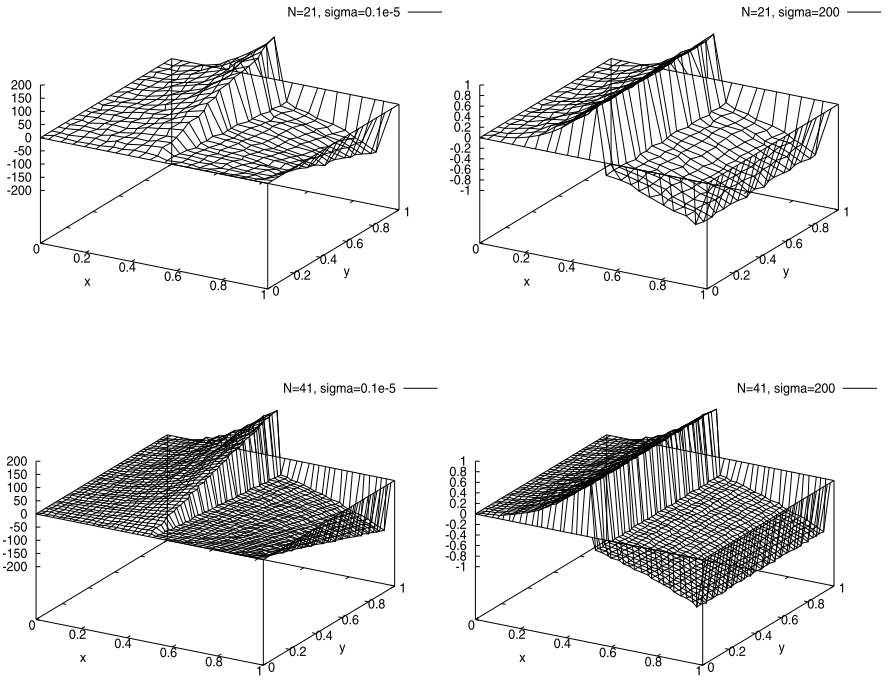

Fig. 14. Numerical approximation obtained with unstructured mesh when $\epsilon = 10^{-6}$, $(b_1, b_2) = (0, 1)$, $\sigma = 10^{-6}, 200$ and $N = 21, 41$.

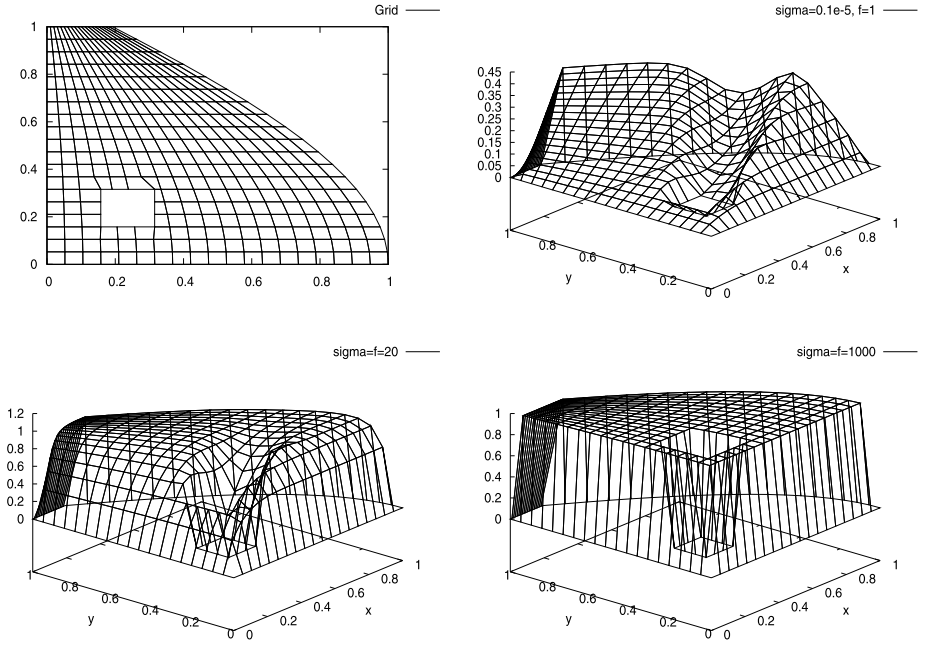

Fig. 15. Numerical approximations when $\epsilon = 10^{-8}$, $(b_1, b_2) = (\cos 20^\circ, \sin 20^\circ)$ with homogeneous Dirichlet boundary conditions.

4.1.8. Experiment 8: non-uniform advection

Next, we consider a test problem which is taken from [20]. The boundary conditions are given by

$$u = \begin{cases} 1, & \text{if } x = 0\,, \;\; 0 \le y \le 1, \\ 0, & \text{otherwise.} \end{cases}$$

We set $\epsilon = 10^{-6}$, $(b_1, b_2) = (y, -x)$, $\sigma = 10^{-6}$, $f = 0$, $N = 41$ and display the numerical results for the proposed method in Fig. 17. The plots show that the present strategy has a potential to solve the problems with variable coefficients. We note

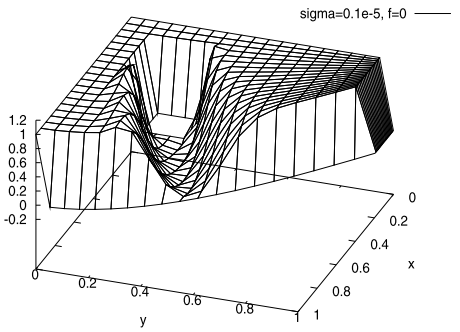

Fig. 16. Numerical approximations when $\epsilon = 10^{-8}$, $(b_1, b_2) = (\cos 20^\circ, \sin 20^\circ)$ with non-homogeneous boundary conditions.

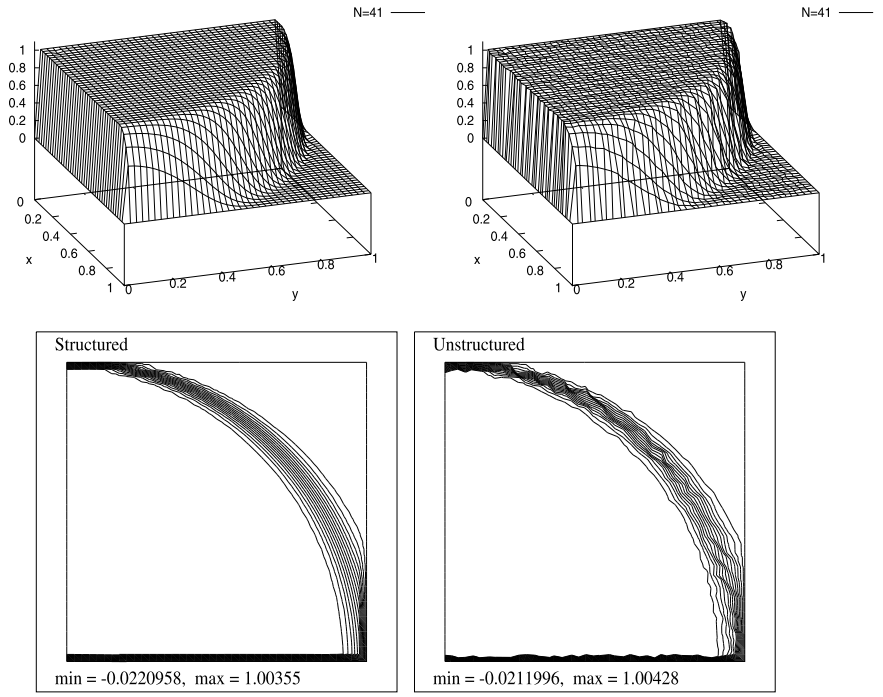

Fig. 17. Numerical approximations obtained with structured and unstructured meshes when $\epsilon = 10^{-6}$, $(b_1, b_2) = (y, -x)$, $\sigma = 10^{-6}$, $f = 0$ and $N = 41$ and the corresponding contour plots.

that the subgrid nodes in the LCB strategy [5] are constructed under the assumption that $\beta \geq 0$ and the whole discussion is applicable to the case $\beta < 0$ as well, by just exchanging the roles of x_1 and x_2 (and consequently of z_1 and z_2).

4.2. Numerical experiments for 3-D CDR problem

4.2.1. Experiment 1

Now, we consider the unit cube subject to the following boundary conditions:

$$u = \begin{cases} 1, & \text{on } (x, y, z = 0); \\ 0, & \text{on the rest of the boundary.} \end{cases}$$

We set $\epsilon = 10^{-6}$, $(b_1, b_2, b_3) = (1, 1, 1)$, $\sigma = 10^{-6}$, $f = 0$ and present elevation plots of the solutions obtained with the present method in Fig. 18. The corresponding contour plots are reported in Fig. 19.

In Fig. 20–21, we test the problem on unstructured grid for the same problem parameters. The numerical solutions show that the method is robust as the results are consistent with the physical configuration of the problem on both structured and unstructured grid.

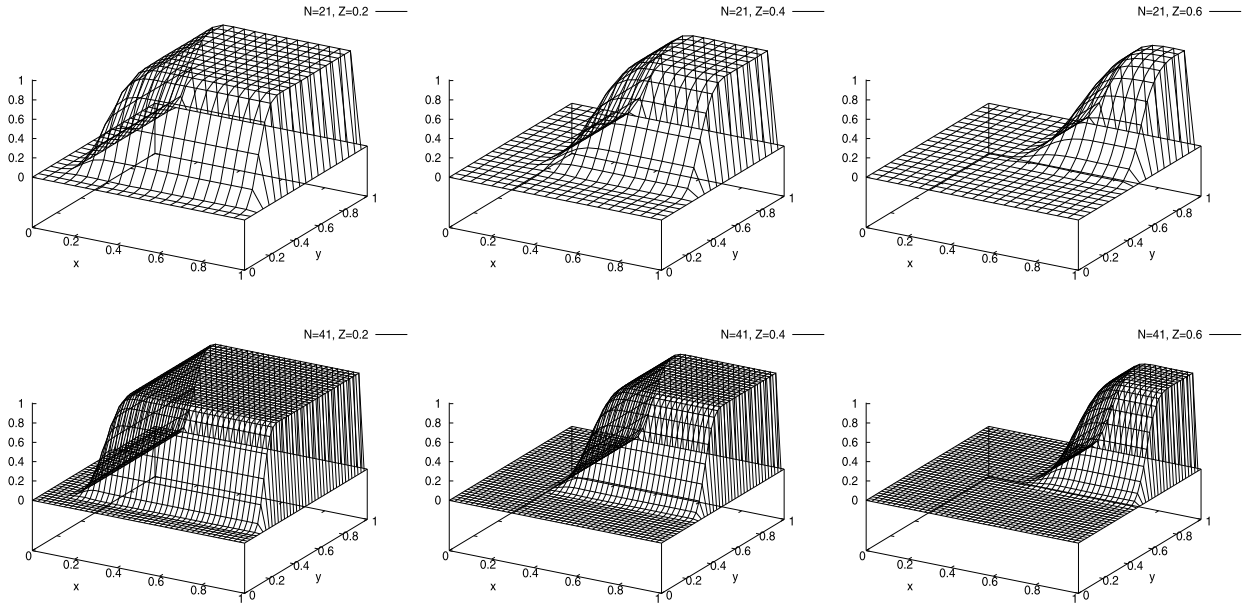

Fig. 18. Numerical approximations obtained with structured mesh when $\epsilon = 10^{-6}$, $(b_1, b_2, b_3) = (1, 1, 1)$, $\sigma = 10^{-6}$ and $N = 21, 41$ at the cuts $z = 0.2$, $z = 0.4$, $z = 0.6$ where $Pe = 25\sqrt{3} \times 10^3$, $Da = \frac{10^{-7}}{2\sqrt{3}}$ (first row) and $Pe = 125\sqrt{3} \times 10^2$, $Da = \frac{10^{-7}}{4\sqrt{3}}$ (second row).

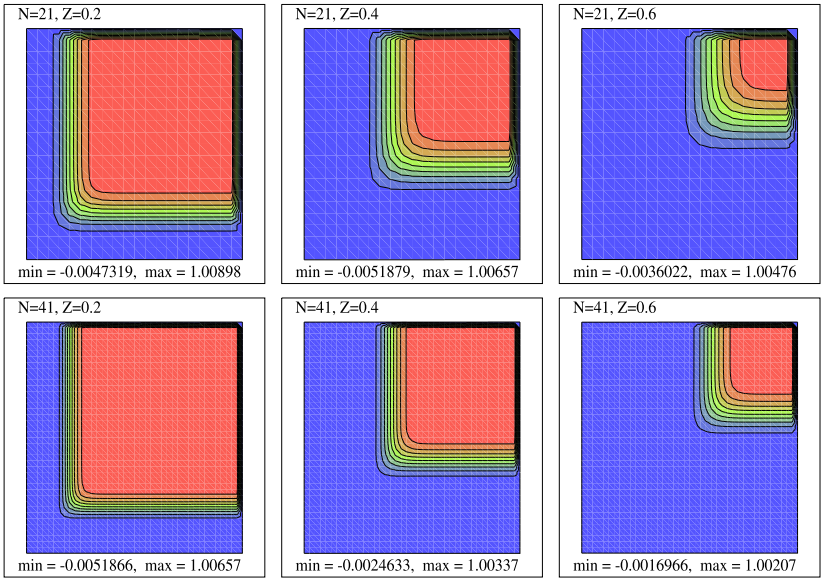

Fig. 19. The corresponding contour plots of Fig. 18.

4.2.2. Experiment 2

Finally, we consider a test problem with variable source function and homogeneous Dirichlet boundary conditions. We set $\epsilon = 10^{-6}$, $(b_1, b_2, b_3) = (1, 1, 1)$, $\sigma = 1000$, $f = 1000x^2y^2z^2$ and display the elevation plots of the solutions obtained with the present method in Fig. 22. The corresponding contour plots are reported in Fig. 23.

In this section, several numerical examples exhibiting boundary/internal layers are given to illustrate the performance and the robustness of the proposed method on both structured and unstructured grids. We also considered the variable discontinuous source function and variable problem parameters and obtained effective results. In order to show the applicability of the method in complex domains, we tested it in a half curved domain for different intensities of reactions. We report that, in all cases, the numerical results are in a good agreement with the exact solution for a wide range of problem parameters, even on coarse meshes and therefore the proposed algorithm is a promising tool to solve CDR problems in any dimensions.

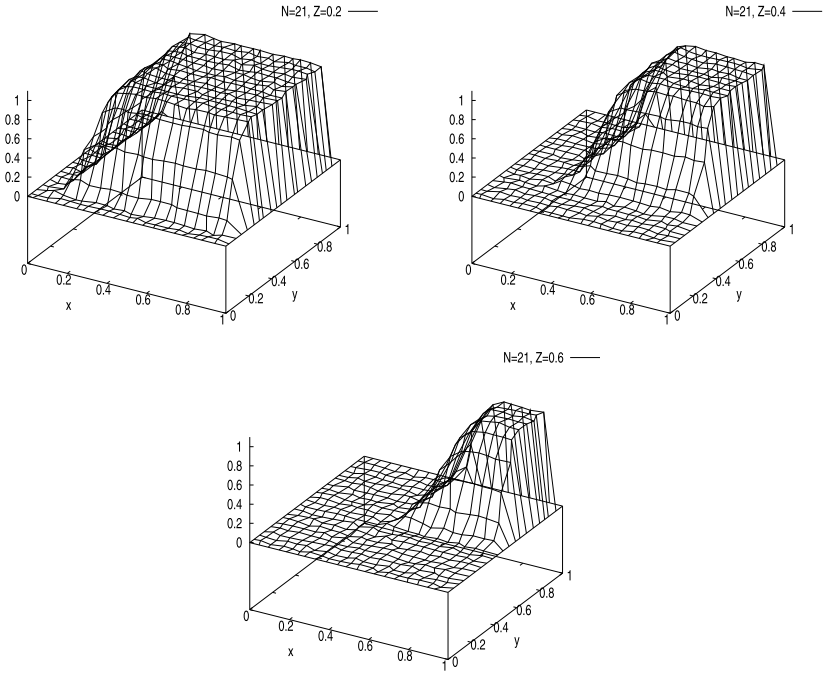

Fig. 20. Numerical approximations obtained with unstructured mesh when $\epsilon = 10^{-6}$, $(b_1, b_2, b_3) = (1, 1, 1)$ and $\sigma = 10^{-6}$ and $N = 21$ at the cuts $z = 0.2$, $z = 0.4$, $z = 0.6$.

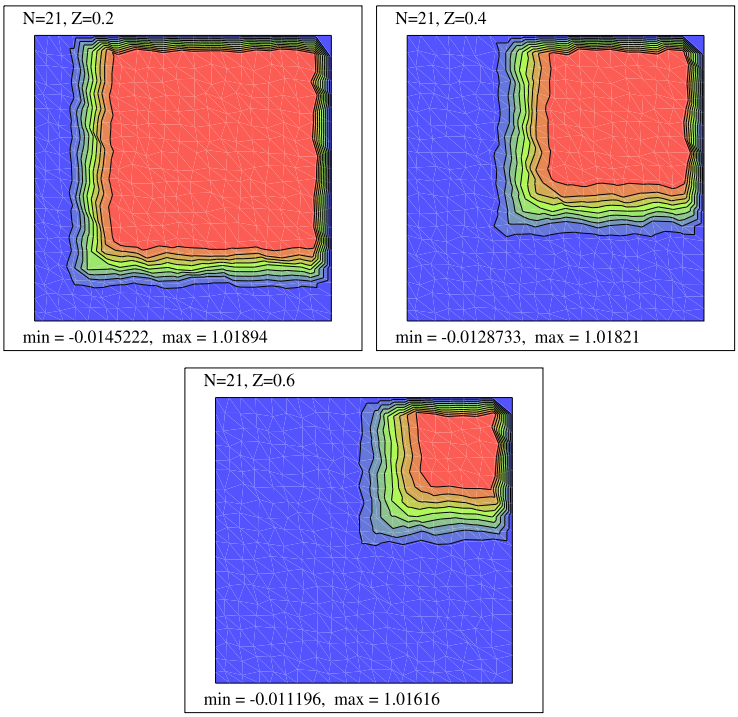

Fig. 21. The corresponding contour plots of Fig. 20.

5. Conclusion

We present a finite difference method for solving the convection–diffusion–reaction problems particularly designed to treat the most interesting case of small diffusion. Numerical results are in a good agreement with the exact solution for a wide range of problem parameters, even when the mesh is coarse and the transition from one regime to another is

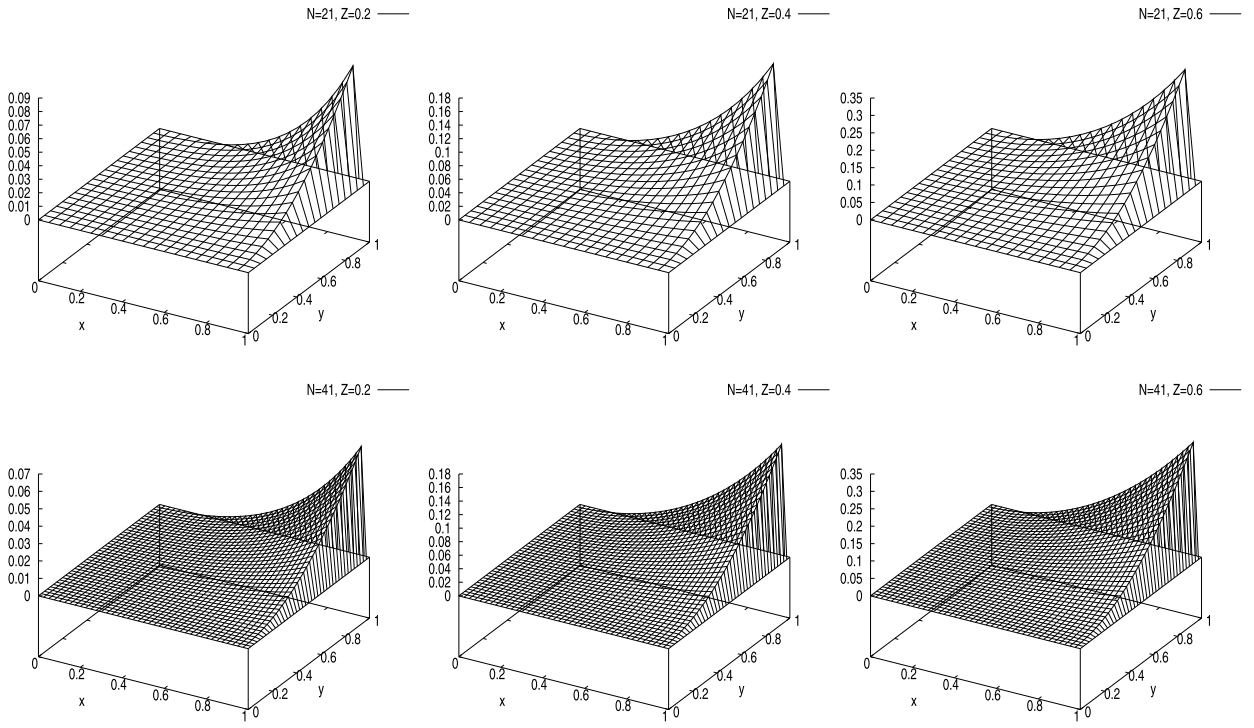

Fig. 22. Numerical approximations obtained with structured mesh when $\epsilon = 10^{-6}$, $(b_1, b_2, b_3) = (1, 1, 1)$, $\sigma = 1000$, $f = 1000x^2y^2z^2$ and $N = 21, 41$ at the cuts $z = 0.2$, $z = 0.4$, $z = 0.6$ where $Pe = 25\sqrt{3} \times 10^3$, $Da = \frac{50}{\sqrt{3}}$ (first row) and $Pe = 125\sqrt{3} \times 10^2$, $Da = \frac{25}{\sqrt{3}}$ (second row).

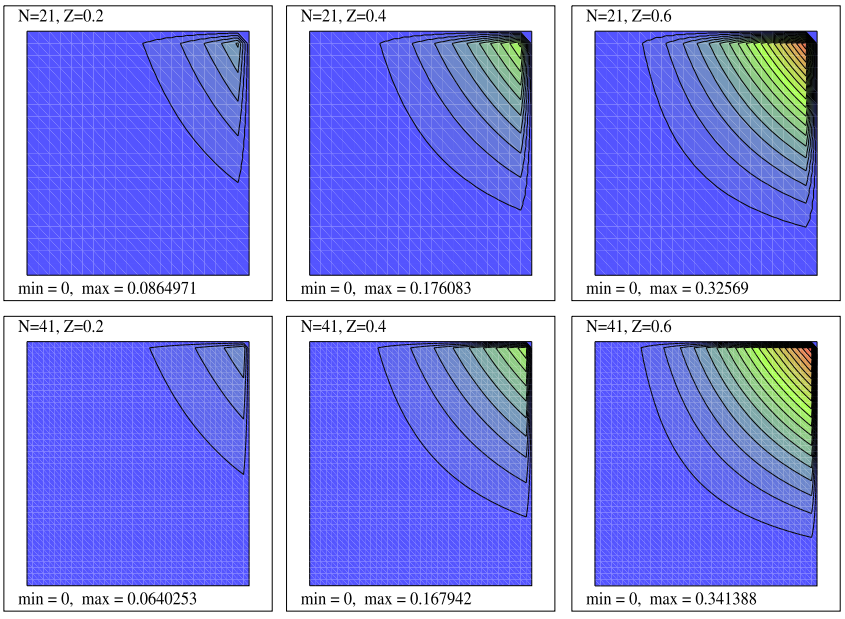

Fig. 23. The corresponding contour plots of Fig. 22.

accurately captured by the algorithm. The main idea of the proposed methodology is based on a simple splitting of the n-dimensional CDR equation into the sum of "n" 1-dimensional equations and combination of the Link-Cutting Bubble (LCB) concept with the finite difference context which permits a different numerical recipe and also an efficient numerical algorithm for the convection–diffusion–reaction problems. This new technique treats the each directions ($x-$, $y-$, ..., etc.) separately a key characteristic that distinguishes the new method from other techniques. Indeed, we take the internal nodes from the LCB strategy which is only effective for 1-D problems and construct a finite different scheme on a nonuniform

mesh. Such a discretization allows the application of modern algorithms such as meshless method to the present model problem with few modifications only. Several benchmark problems are used to compare the performance of the SUPG, RFB and the present method and the superiority of the present method is confirmed in both convection and reaction-dominated regime. The value of the recent method resides in its applicability to the multi-dimensional cases easily, its potential to work on complex geometries and robustness in each regimes without artificial diffusion and a priori knowledge about the location and nature of the layers. The numerical experiments in 2-D and 3-D shows the robustness of the present strategy in both convection and reaction-dominated regimes which is in fact a very important feature, not only for dealing with the steady problem, but also when considering the unsteady problems.

Acknowledgements

The authors dedicate this work to their supervisor Prof. Dr. Ali ?hsan Nesliturk (Department of Mathematics, Izmir Institute of Technology).

This research was partially done while A. Sendur was at the Department of Mathematics Education, Akdeniz University.

References

[1] D.A. Anderson, J.C. Tannehill, R.H. Pletcher, Computational Fluid Mechanics and Heat Transfer, Hemisphere, Washington, DC, 1984.
[2] M.I. Asensio, A. Russo, G. Sangalli, The Residual-Free Bubble numerical method with quadratic elements, Math. Models Methods Appl. Sci. 14 (2004) 641–661.
[3] A.S. Bakhvalov, On the optimization of methods for solving boundary value problems with boundary layers, Ž. Vyčisl. Mat. Mat. Fiz. 9 (1969) 841–859.
[4] C. Baiocchi, F. Brezzi, L.P. Franca, Virtual bubbles and the GaLS, Comput. Methods Appl. Mech. Eng. 105 (1993) 125–141.
[5] F. Brezzi, G. Hauke, L.D. Marini, G. Sangalli, Link-cutting bubbles for the stabilization of convection–diffusion–reaction problems, Math. Models Methods Appl. Sci. 13 (2003) 445–461.
[6] F. Brezzi, L.D. Marini, A. Russo, Applications of pseudo residual-free bubbles to the stabilization of convection–diffusion problems, Comput. Methods Appl. Mech. Eng. 166 (1998) 51–63.
[7] F. Brezzi, L.D. Marini, A. Russo, On the choice of a stabilizing subgrid for convection–diffusion problems, Comput. Methods Appl. Mech. Eng. 194 (2004) 127–148.
[8] F. Brezzi, A. Russo, Choosing bubbles of advection–diffusion problems, Math. Models Methods Appl. Sci. 4 (1993) 571–587.
[9] F. Brezzi, M.O. Bristeau, L.P. Franca, M. Mallet, G. Roge, A relationship between stabilized finite element methods and the Galerkin method with bubble functions, Comput. Methods Appl. Mech. Eng. 96 (1992) 117–129.
[10] A.N. Brooks, T.J.R. Hughes, Streamline upwind/Petrov–Galerkin formulations for convection dominated flows with particular emphasis on the incompressible Navier–Stokes equations, Comput. Methods Appl. Mech. Eng. 32 (1982) 199–259.
[11] C.J. Budd, G.P. Koomullil, A.M. Stuart, On the solution of convection–diffusion boundary value problems using equidistributed grids, SIAM J. Sci. Comput. 20 (2) (2006) 591–618.
[12] R. Codina, Comparison of some finite element methods for solving the diffusion–convection–reaction equation, Comput. Methods Appl. Mech. Eng. 156 (1998) 185–210.
[13] A. Filiz, A. Nesliturk, A. Sendur, A fully discrete ϵ-uniform method for singular perturbation problems on equidistant meshes, Int. J. Comput. Math. 89 (2012) 190–199.
[14] P.A. Farrell, A.F. Hegarty, J.J.H. Miller, E. O'Riordan, G.I. Shishkin, Robust Computational Techniques for Boundary Layers, Chapman & Hall/CRC Press, Boca Raton, FL, 2000.
[15] L.P. Franca, L. Tobiska, Stability of the residual free bubble method for bilinear finite elements on rectangular grids, IMA J. Numer. Anal. 22 (2002) 73–87.
[16] L.P. Franca, F. Valentin, On an improved unusual stabilized finite element method for the advective–reactive–diffusive equation, Comput. Methods Appl. Mech. Eng. 190 (2000) 1785–1800.
[17] L.P. Franca, A.I. Nesliturk, M. Stynes, On the stability of residual-free bubbles for convection–diffusion problems and their approximation by a two-level finite element method, Comput. Methods Appl. Mech. Eng. 166 (1998) 35–49.
[18] L.P. Franca, S.L. Frey, T.J.R. Hughes, Stabilized finite element methods, I. Application to the advective–diffusive model, J. Comput. Appl. Mech. 95 (1992) 253–276.
[19] L.P. Franca, C. Farhat, Bubble functions prompt unusual stabilized finite element methods, Comput. Methods Appl. Mech. Eng. 123 (1995) 299–308.
[20] J. de Frutos, B. Garcia-Archilla, V. John, J. Novo, An adaptive SUPG method for evolutionary convection–diffusion equations, Comput. Methods Appl. Mech. Eng. 273 (2014) 219–237.
[21] P.P.N. Groen, M. Veldhuizen, A stabilized Galerkin method for convection–diffusion problems, SIAM J. Sci. Stat. Comput. 10 (2) (2006) 274–297.
[22] I. Harari, T.J.R. Hughes, The Galerkin/least squares finite element methods for the reduced wave equation with non-reflecting boundary conditions in unbounded domains, Comput. Methods Appl. Mech. Eng. 98 (1992) 411–454.
[23] G. Hauke, A simple subgrid scale stabilized method for the advection–diffusion–reaction equation, Comput. Methods Appl. Mech. Eng. 191 (2002) 2925–2947.
[24] T.J.R. Hughes, L.P. Franca, G.M. Hulbert, A new finite element formulation for computational fluid dynamics: VIII. The Galerkin/leas-squares method for advective–diffusive equations, Comput. Methods Appl. Mech. Eng. 73 (2) (1989) 173–189.
[25] A. Kaya, A finite difference scheme for multidimensional convection–diffusion–reaction equations, Comput. Methods Appl. Mech. Eng. 278 (2014) 347–360.
[26] A. Kaya, Finite difference approximations of multidimensional unsteady convection–diffusion–reaction equations, J. Comput. Phys. 285 (2015) 331–349.
[27] R.B. Kellog, A. Tsan, Analysis of some difference approximations for a singular perturbation problem without turning points, Math. Comput. 32 (1978) 1025–1039.
[28] W. Layton, B. Polman, Oscillation absorption finite element methods for convection–diffusion problems, SIAM J. Sci. Comput. 17 (6) (2012) 1328–1346.
[29] J.J.H. Miller, E. O'Riordan, G.I. Shishkin, Fitted Numerical Methods for Singular Perturbation Problems, World Scientific, Singapore, New Jersey, London, Hong Kong, 1996.
[30] P. Nadukandi, E. Onate, J. Garcia, A high-resolution Petrov–Galerkin method for the convection–diffusion–reaction problem. Part II-A multidimensional extension, Comput. Methods Appl. Mech. Eng. 213–216 (2012) 327–352.
[31] A.I. Nesliturk, On the choice of stabilizing sub-grid for convection–diffusion problem on rectangular grids, Comput. Math. Appl. 59 (2010) 3687–3699.

[32] H.G. Roos, M. Stynes, L. Tobiska, Robust Numerical Methods for Singularly Perturbed Differential Equations, Springer-Verlag, Berlin, 2008.
[33] H.G. Roos, Robust numerical methods for singularly perturbed differential equations: a survey covering 2008–2012, ISRN Appl. Math. 2012 (2012), http://dx.doi.org/10.5042/2012/379547, ID 379547.
[34] A. Sendur, A.I. Nesliturk, Applications of the pseudo residual-free bubbles to the stabilization of convection–diffusion–reaction problems, Calcolo 49 (2011) 1–19.
[35] A. Sendur, A.I. Nesliturk, A. Kaya, Applications of the pseudo residual-free bubbles to the stabilization of convection–diffusion–reaction problems in 2D, Comput. Methods Appl. Mech. Eng. 277 (2014) 154–179.
[36] G.I. Shishkin, Grid approximation of singularly perturbed parabolic equations with internal layers, Sov. J. Numer. Anal. Math. Appl. Model. 3 (1988) 393–407.
[37] R. Verfurth, Robust a posteriori error estimates for stationary convection–diffusion equations, SIAM J. Numer. Anal. 43 (4) (2006) 1766–1782.
[38] C.T. Wu, H.C. Elman, Analysis and comparison of geometric and algebraic multigrid for convection–diffusion equations, SIAM J. Sci. Comput. 28 (6) (2006) 2208–2228.